A Host Enzyme Reduces Metabolic Dysfunction-Associated Steatotic Liver Disease (MASLD) by Inactivating Intestinal Lipopolysaccharide

Zhiyan Wang[1], Nore Ojogun[2], Yiling Liu[1], Lu Gan[1], Zeling Xiao[1], Jintao Feng[1], Wei Jiang[3], Yeying Chen[1], Benkun Zou[4], Cheng-Yun Yu[1], Changshun Li[1], Asha Ashuo[5], Xiaobo Li[6], Mingsheng Fu[7], Jian Wu[5], Yiwei Chu[1], Robert Munford[8*], Mingfang Lu[1, 9, 10*]

1 Department of Immunology, Key Laboratory of Medical Molecular Virology (MOE, NHC, CAMS), School of Basic Medical Sciences, Department of Trauma-Emergency & Critical Care Medicine, Shanghai Fifth People's Hospital, Fudan University, Shanghai, China

2 Infectious Disease Division, Department of Internal Medicine, University of Texas Southwestern Medical Center, Dallas, TX, USA

3 Department of Rheumatology and Immunology, the Affiliated Hospital of Guizhou Medical University, Guiyang, Guizhou, China

4 BeiGene Institute, BeiGene (Shanghai) Research & Development Co., Ltd

5 Department of Medical Microbiology and Parasitology, MOE/NHC/CAMS Key Laboratory of Medical Molecular Virology, School of Basic Medical Sciences, Fudan University, Shanghai, China

6 Department of Physiology and Pathophysiology, School of Basic Medical Sciences, Fudan University, Shanghai, China

7 Department of Gastroenterology, Shanghai Fifth People's Hospital, Fudan University, Shanghai, China

8 Antibacterial Host Defense Unit, Laboratory of Clinical Immunology and Microbiology, National Institute of Allergy and Infectious Diseases (NIAID), National Institutes of Health (NIH), Bethesda, Maryland, USA

9 MOE Innovative Center for New Drug Development of Immune Inflammatory Diseases, Fudan University, Shanghai, China

10 Shanghai Sci-Tech Inno Center for Infection & Immunity, Shanghai, China.

*Corresponding authors:

Robert Munford, Antibacterial Host Defense Unit, Laboratory of Clinical Immunology and Microbiology, National Institute of Allergy and Infectious Diseases (NIAID), National Institutes of Health (NIH), Bethesda, Maryland, USA

9000 Rockville Pike, Bldg. 33, Bethesda, Maryland, USA, 20892

Tel and Fax: 301-443-5755

robertmunford@gmail.com

Mingfang Lu, Department of Immunology, School of Basic Medical Sciences, Fudan University, Shanghai, China

130 Dong An Road, Fudan University Shanghai Medical College, Mail box 226, Xu Hui District, Shanghai, PRC, 200032

Tel and Fax:86-21-54237751

mingfanglu@fudan.edu.cn

Short title: AOAH reduces MASLD

Funding sources: This work was supported by the National Natural Science Foundation of China (32370979, 32170929, 91742104, 31770993 and 31570910 to M. Lu, 32260189, 32300772 to W. Jiang, 82301980 to B. Zou), the Shanghai Committee of Science and Technology (21ZR1405400 to M. Lu), Guizhou Provincial Science and Technology Projects (ZK2024 - 240 to W. Jiang), Science and Technology Program of the Health Commission of Guizhou Province (gzwkj2023-568 to W. Jiang) and National Institutes of Health (AI18188 and AI44642 to R. Munford).

The authors declare that they have no conflicts of interest with the contents of this article.

Abbreviations

AOAH, Acyloxyacyl Hydrolase; LPS, Lipopolysaccharide; MASLD, Metabolic Dysfunction-Associated Steatotic Liver Disease; HFD, High Fat Diet; NC, Normal Chow; PAMP, Pathogen-Associated Molecular Pattern; DAMP, Danger-Associated Molecular Pattern; FA, Fatty Acid; flSREBP1, full-length Sterol Regulatory Element-Binding Protein 1; nSREBP1, nuclear SREBP1; LAM, Lipid-Associated Macrophages; KCs,

Kupffer cells; Mo-KCs, Monocyte-derived Kupffer Cells.

Abstract

The incidence of Metabolic Dysfunction-Associated Steatotic Liver Disease (MASLD) has been increasing world-wide. Since gut-derived bacterial lipopolysaccharides (LPS) can travel via the portal vein to the liver and play an important role in producing hepatic pathology, it seemed possible that (1) LPS stimulates hepatic cells to accumulate lipid, and (2) inactivating LPS can be preventive. Acyloxyacyl hydrolase (AOAH), the eukaryotic lipase that inactivates LPS and oxidized phospholipids, is produced in the intestine, liver, and other organs. We fed mice either normal chow or a high-fat diet for 28 weeks and found that *Aoah*$^{-/-}$ mice accumulated more hepatic lipid than did *Aoah*$^{+/+}$ mice. In young mice, before increased hepatic fat accumulation was observed, *Aoah*$^{-/-}$ mouse livers increased their abundance of Sterol Regulatory Element-Binding Protein 1 (SREBP1) and the expression of its target genes that promote fatty acid synthesis. *Aoah*$^{-/-}$ mice also increased hepatic expression of CD36 and Fabp3, which mediate fatty acid uptake, and decreased expression of fatty acid oxidation-related genes Acot2 and Ppar-α. Our results provide evidence that increasing AOAH abundance in the gut, bloodstream and/or liver may be an effective strategy for preventing or treating MASLD.

Keywords: Metabolic Dysfunction-Associated Steatotic Liver Disease (MASLD), Acyloxyacyl Hydrolase (AOAH), Lipopolysaccharide (LPS), Sterol Regulatory Element-Binding Protein 1 (SREBP1), Gut-Liver Axis

Introduction

Metabolic Dysfunction-Associated Steatotic Liver Disease (MASLD) is a common human affliction. Its global prevalence, currently about 25%, has been increasing (Diehl and Day, 2017; Fan et al., 2017; Younossi et al., 2018). MASLD may progress from nonalcoholic fatty liver to nonalcoholic steatohepatitis, cirrhosis and even hepatic cancer (Friedman et al., 2018; Sheka et al., 2020). Multiple factors may contribute to its pathogenesis (Friedman et al., 2018); prominent among these are the lipopolysaccharides (LPSs, endotoxins) produced by many of the Gram-negative bacteria that inhabit the intestine. Gut-derived LPS may translocate into the portal venous system and traffic to the liver, triggering or exacerbating hepatic inflammation (Albillos et al., 2020; Carpino et al., 2020; Han et al., 2021; Kazankov et al., 2019; Leung et al., 2016; Munford, 1978; Wang et al., 2022).

The LPS molecules that contribute to MASLD pathogenesis are able to stimulate host cells because their lipid A structure is recognized by MD-2/TLR4 receptors (Ye et al., 2012). Most γ-*Proteobacteria* such as *E. coli* produce stimulatory hexaacyl LPS (with six acyl chains) while *Bacteroidetes* produce non-stimulatory LPS that has four or five acyl chains (Anhe et al., 2021; d'Hennezel et al., 2017). MASLD is often associated with intestinal dysbiosis produced by increased abundance of γ-*Proteobacteria*, which leads to tissue inflammation and increased intestinal permeability that allows even more gut-derived LPS to reach the liver (Albillos et al., 2020; Aron-Wisnewsky et al., 2020a; Aron-Wisnewsky et al., 2020b; Mouries et al., 2019; Rodrigues et al., 2024). Although

gut-derived LPS is known to induce hepatic inflammation and to exacerbate MASLD, how LPS influences hepatocyte fatty acid metabolism before MASLD develops has not been well understood.

Acyloxyacyl hydrolase (AOAH) is a highly conserved animal lipase that is mainly expressed in macrophages, monocytes, neutrophils, microglia, dendritic cells, NK cells and ILC1 cells (Munford et al., 2020). It can inactivate Gram-negative bacterial LPSs by releasing two of the six fatty acyl chains present in the lipid A moiety (Figure 1A). It also can deacylate/inactivate oxidized phospholipids and lysophospholipids, molecules that are also known to contribute to MASLD (Sun et al., 2020; Zou et al., 2021). We previously reported that AOAH is expressed by gut macrophages and dendritic cells and can inactivate bioactive LPS in feces (Cheng et al., 2023; Janelsins et al., 2014; Qian et al., 2018). AOAH also inactivates LPS in the liver, diminishing and shortening hepatic inflammation induced by bloodborne LPS (Ojogun et al., 2009; Shao et al., 2011; Shao et al., 2007). Han et al. found that intestine-derived LPS can bind high-density lipoprotein 3 (HDL_3) and be inactivated by AOAH as it traffics from the jejunum to the liver via the portal vein (Han et al., 2021). The enzyme's ability to prevent MASLD by inactivating gut-derived LPS had not been tested (Ojogun, 2008).

In this study, we found that when mice were fed either normal chow or a high fat diet, AOAH reduced LPS-induced lipid accumulation in the liver, probably by decreasing the expression and activation of Sterol Regulatory Element-Binding Protein 1 (SREBP1), an important transcription factor that promotes fatty acid synthesis (Horton et al., 2002;

Shimano and Sato, 2017). AOAH also reduced the expression of CD36 and Fabp3, fatty acid uptake-related genes, and increased that of fatty acid oxidation-related genes (Acot2 and Ppar-α). In addition, AOAH reduced hepatic inflammation and minimized tissue damage. Our results suggest that AOAH plays a regulatory role in ameliorating MASLD and suggest that measures that increase AOAH abundance in the intestine, liver and/or bloodstream may help prevent this common disease.

Materials and methods

Mice

C57BL/6J *Aoah*$^{-/-}$ mice were produced at the University of Texas Southwestern Medical Center, Dallas, Texas (Lu et al., 2003), transferred to the National Institutes of Health, Bethesda, Maryland, USA, and then provided to Fudan University, Shanghai, China. The mutated *Aoah* gene had been backcrossed to C57BL/6J mice for at least 10 generations. *Aoah*$^{+/+}$ and *Aoah*$^{-/-}$ male mice were housed in a specific pathogen-free facility with 12-h light/dark cycle at 22 °C in Fudan University Experimental Animal Center (Shanghai, China). *Aoah*$^{+/+}$ and *Aoah*$^{-/-}$ male mice were co-housed for at least 3 weeks before the start and throughout the experiments. All studies used protocols approved by the Institutional Animal Care and Use Committee (IACUC) of Fudan University (2023-DWYY-03JZS). All animal study protocols adhered to the Guide for the Care and Use of Laboratory Animals.

The MASLD mouse model

Co-housed *Aoah*$^{+/+}$ and *Aoah*$^{-/-}$ male mice were fed either a normal diet (NC) or a high fat calorie diet (D12492, Research Diets, USA) that contained protein: carbohydrate: fat (20:20:60, kcal%) plus high fructose (23.1 g/L; F3510, Sigma,USA) and glucose (18.9 g/L; G8270, Sigma, USA) in the drinking water (HFD) for 28 weeks (Liu et al., 2018).

Blood analysis

Total triacylglycerol, total cholesterol, low density lipoprotein (LDL), high-density lipoprotein (HDL), aspartate aminotransferase (AST) and alanine aminotransferase (ALT) in mouse serum were measured in the Department of Laboratory Animal Science, Fudan University using ADVIA Chemistry XPT.

Liver histology

After livers were excised and fixed in 4% paraformaldehyde for 18 h, they were sectioned and stained with hematoxylin and eosin (H & E) and Oil Red O. The samples were examined for steatosis, hepatocyte ballooning degeneration, lobular inflammation and lipid droplets using a Nikon E200 microscope.

MASLD activity score

Histological analysis of the liver was performed based on the Sheka MASLD scoring criteria (Sheka et al., 2020). Liver steatosis is an infiltration of hepatic fat with minimal inflammation and is graded based on the fat percentage in hepatocytes: grade 0 (< 5%), grade 1 (5% – 33%), grade 2 (33% – 66%), and grade 3 (> 66%). Inflammatory activity is manifested by two factors: grade 0 (no inflammation), grade 1 (< 2 foci per 200 × field), grade 2 (2 – 4 foci per 200 × field), grade 3 (> 4 foci per 200 ×

field), and the presence of hepatocyte ballooning degeneration: no ballooned cells (grade 0), a few ballooned cells (grade 1), and many ballooned cells (grade 2).

Liver lipid analysis

Undiluted serum samples and liver homogenates (50 mg/ml) were run in duplicate alongside a standard curve of glycerol (triglyceride assay), cholesterol (cholesterol assay) or palmitic acid (free fatty acid assay) according to the manufacturer's instructions. Triglyceride Determination Kit and Cholesterol Determination Kit were obtained from Applygen. Free Fatty Acid Quantitation Kit was purchased from Sigma-Aldrich.

Quantitative Real - time PCR (qPCR)

RNA from livers or isolated hepatocytes was purified using TRNzol Universal Reagent (Tiangen) and reversely transcribed (Tiangen). The primers used for qPCR are listed in Table S1. Actin was used as an internal control and the relative gene expression was calculated using the ΔΔCt quantification method.

Liver immune cell isolation

After mice were exsanguinated, 2 ml PBS containing collagenase (5 mg/ml, type IV, Sigma) were injected into the liver via the inferior vena cava. The liver was cut into small pieces and treated with collagenase (0.5 mg/ml) for 10 min at 37 °C. The liver pieces were mashed by using syringe plungers. The cells were passed through a 70 μm strainer (WHB scientific) and then centrifuged at 50 g for 3 min, 3 times, to pellet hepatocytes. The immune cells in the supernatant were pelleted (500 g for 15 min) and then isolated on a 40% Percoll step gradient (Cytiva). The cells were then stained and

analyzed using flow cytometry (Shao et al., 2007).

Flow cytometry

Liver cells were collected by centrifugation and then incubated with Fc blocking antibody (purified anti-mouse CD16/32, BioLegend) on ice for 15 min. After the cells were stained with fluorescence-conjugated antibodies for 30 min on ice, they were washed and subjected to FACS (BD, FACSCelesta). The FACS data were analyzed using Flow Jo software (TreeStar,Inc). All antibodies used for flow cytometry were anti-mouse antigens. Anti-mouse antibodies used for flow cytometry were anti-CD45-BV785 (Clone 30-F11, BioLegend), anti-CD11b-FITC (Clone M1/70, BioLegend), anti-F4/80-BV421 (Clone BM8, BioLegend), anti-Ly6G-PerCP-Cy5.5 (Clone 1A8, BioLegend), anti-Ly6C-APC-Cy7 (Clone HK1.4, BioLegend), anti-MHC II-PE-Cy7 (Clone M5/114.15.2, BioLegend), anti-VSIG4-APC (Clone NLA14, eBioscience), and anti-Tim4-PE (Clone RMT4-54, BioLegend).

Hepatocyte isolation

Primary hepatocytes were isolated from adult mice using a two-step collagenase perfusion method (Charni-Natan and Goldstein, 2020). In brief, the peritoneal cavity was opened and the liver was perfused *in situ* via the portal vein at 37°C with 20 ml PBS followed by 20 ml DMEM containing 10 mg collagenase (type IV, Sigma). The liver was then removed and gently minced, and the released cells were dispersed in DMEM containing 5% fetal bovine serum (FBS) and 1% penicillin/streptomycin. The solution containing the mixed cells and debris was passed through a 100 μm cell strainer, and then

centrifuged at 50 g for 3 min, twice. The hepatocytes were pelleted and then isolated on a 90% Percoll step gradient (Cytiva). Hepatocytes were then resuspended in a TRNzol Universal Reagent (Tiangen) to measure mRNA.

Western blot

Small pieces of liver were lysed with RIPA buffer (Biyotime) containing 1 mM PMSF (Biyotime) and a proteinase inhibitor mixture (Selleck). A commercial cytosol and nucleus Protein Extraction Kit (P0027, Beyotime) was used to separate cytosolic and nuclear proteins in the liver. The following antibodies were used for Western blot analysis: anti-SREBP1 (SC-17755, Santa cruz), anti-AOAH (HPA021666; Sigma-Aldrich), anti-Lamin B1 (12987-1-AP, Proteintech), anti-SCD1 (ab39969, Abcam), anti-FASN (SC-48357, Santa cruz), anti-Phospho-mTOR (Ser2448) (5536, Cell Signaling Technology), anti-Phospho-p70 S6 Ribosomal Protein (Thr389) (9234, Cell Signaling Technology), anti-Phospho-AKT (Ser473) (4060, Cell Signaling Technology), anti-Phospho-mTOR (Ser2448) (5536, Cell Signaling Technology), anti-mTOR (2983, Cell Signaling Technology), anti-p70 S6 Ribosomal Protein (2217, Cell Signaling Technology), anti-AKT (4691, Cell Signaling Technology), and anti-α-Tublin (HRP-66031; Proteintech). HRP-linked anti-mouse IgG (7076S; Cell Signaling Technology) and HRP-linked anti-rabbit IgG (7074S, Cell Signaling Technology) were used as secondary antibodies. ECL substrate (Bio-Rad Diagnostic) was used to detect proteins in Western blotting and the blot bands were quantified by using Image J.

Measurement of TLR4-stimulating activities in mouse feces, liver and plasma

Fresh feces were collected and resuspended in endotoxin-free PBS (0.1 g/ml) and centrifuged at 800 g for 5 min. The supernatant was heated at 70 °C for 10 min. Mice were bled from the eye socket; 5 μl of 0.5 M EDTA was used as an anti-coagulant. Livers were homogenized in PBS, centrifuged and the supernatant was obtained. In some experiments, 200 μg of LPS was resuspended in 200 μl of PBS and then the suspension was slowly administered into the esophagus of mice using a gavage needle. Twenty-four h later, the livers were collected for analysis. All the samples were collected for TLR4-stimulating activity using a cell-based colorimetric endotoxin detection kit (HEK-Blue LPS Detection Kit2, InvivoGen). Diluted samples were added to human embryonic kidney (HEK-293) cells that expressed hTLR4 and a NF-κB-inducible secreted embryonic alkaline phosphatase reporter gene. After 18 h incubation, cell culture media were applied to QUANTI-Blue medium to measure alkaline phosphatase activity. A preparation of *E. coli* 055:B5 LPS, standardized to FDA-approved control standard endotoxin, which was included in the kit, was used to quantitate TLR4-stimulating activity. Plates were read at a wavelength of 620 nm (Tecan).

Gut permeability analysis

After mice were fasted for 18 h, they were orally gavaged with fluorescein isothiocyanate (FITC) -conjugated 4 kDa dextran (50 mg per 100 g body weight) (46944, Sigma-Aldrich). Four hours after gavage, blood was collected from the facial vein and the serum was used for FITC fluorescence measurements (excitation, 490 nm; emission,

520 nm).

RNA-sequencing analysis

Total RNA was isolated using TRNzol from co-housed 6 - 8 weeks old *Aoah*$^{+/+}$ and *Aoah*$^{-/-}$ mouse livers. The libraries were sequenced on an Ilumina Novaseq 6000 platform and 150 bp paired-end reads were generated. Differential expression analysis was performed using the DESeq2. Q value < 0.05 and foldchange > 1.5 was set as the threshold for significantly differential gene expression. Gene Set Enrichment Analysis (GSEA) was performed using GSEA software. RNA-seq analysis was conducted by Shanghai OE Biotech. Co., Ltd. China and the results were deposited at PRJNA1022016.

Single-cell RNA sequencing analysis

AOAH expression in mouse hepatic cells was analyzed based on single cell RNAseq data using the Liver Cell Atlas at https://www.livercellatlas.org/ (Remmerie et al., 2020). Liver single-cell RNA sequencing data from MASLD-cirrhosis patients (n = 5) and healthy controls (n = 5) were obtained from GSE136103 (Ramachandran et al., 2019). R package Seurat (version 5.1.0) was utilized for clustering and cell type identification.

Kupffer cell deletion

Kupffer cells were depleted by injecting 200 μl Clodronate-liposomes (Liposoma BV) i.v. and PBS-liposomes were used as controls. Two days after injection, Kupffer cell deletion was confirmed by staining F4/80^{+} cells in cryostat liver sections.

Statistical analysis

Data were presented as mean ± SEM. Differences between groups were analyzed

using Mann-Whitney test. To compare kinetic difference, two-way ANOVA test was used. The statistical significance was set at $P < 0.05$. *, $P < 0.05$; **, $P < 0.01$; ***, $P < 0.001$.

Results

AOAH reduces hepatic lipid accumulation.

To find out if AOAH prevents MASLD, we fed co-housed *Aoah*$^{+/+}$ and *Aoah*$^{-/-}$ mice Normal Chow (NC) or a High Fat Diet (HFD) plus fructose and glucose in the drinking water, for 28 weeks (Figure 1B) (Liu et al., 2018). *Aoah*$^{-/-}$ mice fed either NC or HFD gained more weight than did *Aoah*$^{+/+}$ control mice (Figure 1C). When they were fed either NC or HFD, the livers of *Aoah*$^{-/-}$ mice were heavier than those of *Aoah*$^{+/+}$ control mice (Figure 1D). Histological examination and Oil Red O staining revealed that *Aoah*$^{-/-}$ mouse livers accumulated more lipid droplets than did the livers of *Aoah*$^{+/+}$ mice (Figure 1E). When we scored MASLD severity based on steatosis, hepatocyte ballooning degeneration and inflammation, *Aoah*$^{-/-}$ mice developed more severe MASLD than did *Aoah*$^{+/+}$ mice whether the mice were fed NC or HFD (Sheka et al., 2020) (Figure 1E). When the mice were fed either NC or HFD, *Aoah*$^{-/-}$ mouse livers contained more triacylglycerol (TAG) than did *Aoah*$^{+/+}$ mouse livers, while livers from both mouse strains contained a similar amount of total cholesterol (TCHO, Figure 1F). When the mice were fed the HFD, *Aoah*$^{-/-}$ mice had higher serum levels of triacylglycerol, total cholesterol, low density lipoprotein (LDL) and free fatty acids than did *Aoah*$^{+/+}$ mice

(Figure 1G). Collectively, these findings were evidence that AOAH reduced hepatic triacylglycerol accumulation when mice were fed either NC or HFD.

AOAH prevents hepatic inflammation and tissue injury when mice are fed HFD.

Aoah$^{-/-}$ mice fed HFD had significantly higher serum alanine aminotransferase (ALT) and aspartate aminotransferase (AST) levels than did control *Aoah*$^{+/+}$ mice, suggesting that *Aoah*$^{-/-}$ mice experienced more severe liver inflammation and tissue damage (Figure 2A). To assess liver inflammation, we measured pro- and anti-inflammatory cytokine expression. When mice were fed the HFD, *Aoah*$^{-/-}$ mouse livers produced more pro-inflammatory IL-6, IFN-γ and anti-inflammatory IL-10 mRNA than did *Aoah*$^{+/+}$ mouse livers, suggesting greater inflammation (Figure 2B). We also found that *Aoah*$^{-/-}$ livers had more Timp1 (a pro-fibrosis gene) mRNA and less MMP2 (an anti-fibrosis gene) mRNA than did *Aoah*$^{+/+}$ mouse livers (Kisseleva and Brenner, 2021), indicating that *Aoah*$^{-/-}$ mouse livers may be developing more severe fibrosis, although we did not detect fibrosis with Masson staining (Figure 2C). We analyzed the myeloid cells in the liver (Daemen et al., 2021) and found that when the mice were fed the HFD, *Aoah*$^{-/-}$ mouse livers contained more neutrophils, monocytes and lipid-associated macrophages (hepatic LAMs) (Remmerie et al., 2020; Su, 2002) than did *Aoah*$^{+/+}$ mouse livers (Figure 2D, E). Collectively, when the mice were fed a HFD, the livers of *Aoah*$^{-/-}$ mice developed significantly greater inflammatory responses and tissue damage.

AOAH reduces hepatic LPS levels and the expression of fatty acid synthesis genes.

We found previously that AOAH was mainly expressed in Kupffer cells in the liver (Shao et al., 2007). To confirm the previous results, we first consulted the single cell RNAseq analysis reported by Remmerie et al. (Remmerie et al., 2020), who found that AOAH is expressed in Kupffer cells, monocytes, monocyte-derived cells, NK (circulating NK) and ILC1 (tissue resident NK) cells in mouse livers (Remmerie et al., 2020) (Figure 3A). We used flow cytometry to sort mouse Kupffer cells ($CD45^{+}NK1.1^{-}$ $F4/80^{hi}CD11b^{mid}$), monocytes ($CD45^{+}NK1.1^{-}$ $F4/80^{mid}CD11b^{hi}$), NK cells ($CD45^{+}SSC^{lo}$ $NK1.1^{+}$) (including circulating NK and resident ILC1) and we purified the hepatocytes. Using qPCR analysis, we found that AOAH mRNA was present in Kupffer cells, monocytes and NK cells but not in hepatocytes, in keeping with previous findings (Shao et al., 2007) (Figure 3B). Western blot analysis confirmed that *Aoah*$^{+/+}$ mouse livers but not *Aoah*$^{-/-}$ mouse livers had AOAH protein (Figure 3C). When *Aoah*$^{+/+}$ mice aged or had a high fat diet, their hepatic AOAH expression increased (Figure 3D). We also studied the expression of AOAH in human liver cells by analyzing the single-cell RNAseq data obtained by Ramachandran et al. (Ramachandran et al., 2019); AOAH was expressed in macrophages, monocytes, resident and circulating NK cells, and some T cells (Figure 3E). AOAH expression increased in liver macrophages and monocytes in MASLD patients (Figure 3E). As gut-derived LPS can be transported via the portal vein into the liver (Han et al., 2021), we hypothesized that AOAH prevents hepatic inflammation and fat accumulation by inactivating LPS in the gut, portal vein, and liver.

We found that *Aoah*$^{-/-}$ mouse feces, liver and plasma had higher bioactive LPS levels when *Aoah*$^{-/-}$ and *Aoah*$^{+/+}$ mice were fed either NC or HFD (Figure 3F). HFD increased gut permeability, but there was no permeability difference between *Aoah*$^{+/+}$ and *Aoah*$^{-/-}$ mice that were fed either NC or HFD for 28 weeks, suggesting that the increased hepatic LPS levels in *Aoah*$^{-/-}$ mouse livers was mainly caused by failure to inactivate LPS (Figure 3G). After the mice were fed HFD for 28 weeks, *Aoah*$^{-/-}$ mouse livers increased fatty acid uptake gene *Fabp3* mRNA and fatty acid synthesis gene *Fasn* mRNA, changes that may have contributed to lipid accumulation (Figure 3H). Thus, AOAH may prevent hepatic lipid accumulation by diminishing bioactive LPS in the liver.

AOAH can regulate the expression of hepatic fatty acid metabolism genes.

We found that AOAH reduced hepatic lipid accumulation when mice were about 8 months old if they were fed either NC or HFD. To investigate the mechanism, we analyzed the livers of young mice. We co-housed 3 - 4 - week - old *Aoah*$^{+/+}$ and *Aoah*$^{-/-}$ mice for 3 - 4 more weeks before removing their livers for RNAseq analysis. The expression of several fatty acid biosynthesis genes, such as Acacb (acetyl-Coenzyme A carboxylase beta), Acss2 (Acetyl-CoA synthetase 2), Pcx (Pyruvate carboxylase), Acly (ATP citrate lyase), Fasn (Fatty acid synthase) and Scd1 (Stearoyl-Coenzyme A desaturase 1), was significantly increased in *Aoah*$^{-/-}$ mouse livers (Figure 4A). When we used GSEA (Gene set enrichment analysis) to analyze deferentially expressed genes, we found that the fatty acid biosynthesis pathway was enriched (Figure 4B). We then did

qPCR and confirmed the increases in mRNAs for FA biosynthesis genes described in Figure 4A as well as for Acaca (acetyl-Coenzyme A carboxylase alpha, encoding ACC1, the first and key enzyme on FA synthesis pathway) in *Aoah*$^{-/-}$ mouse livers compared with *Aoah*$^{+/+}$mouse livers (Figure 4C). In addition, mRNAs for enzymes involved in fatty acid oxidation (Acot2 (Acyl-CoA thioesterase 2) and Ppar-α (peroxisome proliferator-activated receptor α) (Bougarne et al., 2018; Moffat et al., 2014) decreased (Figure 4D), while CD36 (fatty acid uptake (Chen et al., 2022)) mRNA levels increased in *Aoah*$^{-/-}$ mouse livers (Figure 4E). We confirmed that FASN and SCD1 protein levels also increased in *Aoah*$^{-/-}$ mouse livers (Figure 4F). We found previously that LPS and other TLR agonists increase lipid accumulation in cultured macrophages by increasing expression of Acsl1 (Acyl-CoA synthetase long-chain family member 1) and Dgat2 (Diacylglycerol O-acyltransferase 2) and by reducing the production of Atgl (Adipose triglyceride lipase, Pnpla2) (Huang et al., 2014), yet the livers of *Aoah*$^{+/+}$ and *Aoah*$^{-/-}$ mice had similar levels of Acsl1, Dgat2 and Atgl (Pnpla2) mRNA, suggesting that AOAH does not regulate hepatic triacylglycerol metabolism (Figure S1). These results suggest that AOAH reduces liver fat accumulation by diminishing the expression of fatty acid synthesis and uptake genes and increasing that of fatty acid oxidation genes.

AOAH reduces hepatic SREBP1.

As Acaca, Fasn and Scd1 are all target genes for sterol regulatory element-binding protein 1 (SREBP1), a key transcription factor for fatty acid biosynthesis, we next

analyzed SREBP1 expression in the liver (Horton et al., 2002; Shimano and Sato, 2017; Yokoyama et al., 1993). There are two isoforms of SREBP1, SREBP1a and SREBP1c, and the liver predominantly expresses SREBP1c (Horton et al., 2002). The abundance of SREBP-1a and SREBP-1c mRNA increased in the livers of young *Aoah*$^{-/-}$ mice (Figure 5A). SREBP1 is synthesized as a 125 KDa precursor (full length, flSREBP1) in the endoplasm reticulum, transferred to the Golgi apparatus, and cleaved sequentially by Site-1 protease and Site-2 protease to generate nuclear SREBP1 (nSREBP1, 68 KDa), which enters the nucleus and activates fatty acid biosynthesis gene transcription (Horton et al., 2002; Shimano and Sato, 2017). The livers mainly had the short form (68 KDa) nSREBP1 protein, which was significantly more abundant in *Aoah*$^{-/-}$ mice (Figure 5B). We separated liver cytosol and nuclei and found that the short form SREBP1 was mainly present in nuclei and that *Aoah*$^{-/-}$ mouse liver nuclei contained significantly more SREBP1 than did *Aoah*$^{+/+}$ mouse liver nuclei (Figure 5C).

When we analyzed the transcript profiles from co-housed 6 - 8 - week - old *Aoah*$^{+/+}$ and *Aoah*$^{-/-}$ mouse livers, we noticed that the expression of inflammatory genes for serum amyloid A1 (SAA1), SAA2 and SAA3 was significantly higher in *Aoah*$^{-/-}$ mouse livers (Figure S2A). We isolated hepatocytes from *Aoah*$^{+/+}$ and *Aoah*$^{-/-}$ mice and found that *Aoah*$^{-/-}$ mouse hepatocytes expressed increased levels of Saa1, Saa2, Saa3 and inflammation regulatory Irak-m mRNA (Figure S2B). Purified hepatocytes from *Aoah*$^{-/-}$ mice had increased levels of Acly, Acaca, Acacb, Fasn and CD36 mRNA (Figure S2C, D) and decreased levels of Acot2 and Ppar-α mRNA (Figure S2E), changes that may

contribute to lipid accumulation as mice grow older. Thus, in young mice, even before hepatic lipid accumulation can be observed, *Aoah*$^{-/-}$ mouse hepatocytes have altered expression of genes that may promote lipid storage.

We next used clodronate-liposomes to deplete Kupffer cells and found that clodronate-liposome treatment diminished liver AOAH mRNA, confirming that Kupffer cells are the major source of hepatic AOAH (Shao et al., 2007) (Figure 5D). Notably, after clodronate liposome treatment, nSREBP1 levels increased in the liver significantly, resembling *Aoah*$^{-/-}$ mice (Figure 5D). AKT-mTOR1-p70 S6-kinase (S6K) activation induces SREBP1c processing in hepatocytes (Jeon et al., 2023b; Owen et al., 2012; Yecies et al., 2011). Livers from clodronate-liposome treated mice had increased AKT and mTOR activation (Figure 5D), suggesting that when gut-derived LPS cannot be inactivated by AOAH in the liver, bioactive LPS stimulates the mTOR pathway and induces SREBP1 activation.

Excessive gut-derived LPS increases hepatic nSREBP1 and mTOR activation.

To find out if excessive gut LPS increases liver LPS levels and promotes fatty acid synthesis gene expression, we orally gavaged *Aoah*$^{+/+}$ mice with LPS. We confirmed that orally gavaged (*i.g.*) LPS increased hepatic LPS levels in *Aoah*$^{+/+}$ mice (Figure 6A). Like *Aoah*$^{-/-}$ mice, *Aoah*$^{+/+}$ mice that received gavaged LPS had increased levels of Srebp1a, Srebp1c, Pcx, Acaca, Acacb, Fasn, Scd1 and Cd36 mRNA in their livers (Figure 6B, C). LPS administered *i.g.* also increased nSREBP1 in *Aoah*$^{+/+}$ mouse livers (Figure

6D). Consistently, elevated AKT-mTOR-S6K activation was found in *Aoah*$^{-/-}$ mouse livers and when we gave *Aoah*$^{+/+}$ mice i.g. LPS, hepatic AKT-mTOR-S6K activity increased (Figure 6D). To find out whether LPS can directly stimulate hepatocytes to induce SREBP1 activation, we isolated primary hepatocytes and found that LPS stimulated mTOR activation and nSREBP1 upregulation (Figure 6E). Adding purified Kupffer cells to the hepatocyte culture did not further increase SREBP1 activation, suggesting that LPS directly acts on hepatocytes (Yu et al., 2021), at least in vitro. Blocking mTOR activation using torin1 prevented LPS-induced nSREBP1 upregulation (Figure 6E), suggesting that upon LPS stimulation, SREBP1 activation depends upon the mTOR pathway. Collectively, these results confirm that excessive hepatic LPS derived from the *Aoah*$^{-/-}$ mouse intestine induces hepatocyte mTOR activity, which increases nSREBP1 abundance; AOAH prevents hepatic lipid accumulation by inactivating gut-derived LPS.

Discussion

The intestine and liver are connected by the portal vein, enabling the transport of gut commensal-derived molecules, including Gram-negative bacterial LPS, to the liver (Albillos et al., 2020; Leung et al., 2016). Much evidence suggests that gut-derived LPS induces hepatic inflammation and therefore exacerbates MASLD, especially when dysbiosis and intestinal barrier dysfunction have occurred (An et al., 2022; Aron-Wisnewsky et al., 2020a; Aron-Wisnewsky et al., 2020b; Leung et al., 2016). As

lipid accumulation in hepatocytes is considered to be the first hit, gut-derived LPS is usually thought to be the second hit in the pathogenesis of MASLD, mainly inducing inflammation (An et al., 2022), yet the possibility that LPS also has direct effects on hepatocyte lipid metabolism has received little attention. In previous studies we found that when we co-housed *Aoah*$^{+/+}$ and *Aoah*$^{-/-}$ mice for 3 or more weeks, they had similar microbiota (Qian et al., 2018), yet we found significantly more LPS in *Aoah*$^{-/-}$ mouse feces and livers. In this study, we found that *Aoah*$^{-/-}$ mice accumulated more hepatic fat than did *Aoah*$^{+/+}$ mice when the mice were fed either normal chow or a high fat diet. *Aoah*$^{-/-}$ mouse livers also expressed more inflammation-inducing and pro-fibrosis genes and had more liver damage when they were fed a HFD. Notably, when *Aoah*$^{-/-}$ mice were young and had not developed MASLD their livers already expressed significantly elevated levels of nSREBP1 and its target genes (Figure 7).

Liver is an important tissue that converts carbohydrates into lipids (Jeon et al., 2023a). SREBP1c, the predominant isoform expressed in the liver, plays an important role in fatty acid synthesis (Shimano and Sato, 2017); SREBP1c mRNA was elevated in MASLD patient livers (Kohjima et al., 2008) and its chronic activation contributed to MASLD progression (Kawano and Cohen, 2013); SREBP1 has become a target for MASLD treatment (Ju et al., 2020; Jump et al., 2013). Intriguingly, nSREBP1 levels increased in the livers of 6 – 8 weeks old (i.e., young) *Aoah*$^{-/-}$ mice before MASLD developed; the expression of many SREBP1 target genes, such as those involved in fatty acid biosynthesis (Acly, Acaca, Acacb, Fasn, Scd1, Acss2) also increased. In addition,

SREBP1a and SREBP1c mRNA both increased in *Aoah*$^{-/-}$ mouse livers, suggesting that regulation occurs at the transcription level or, because the Srebf1 gene (encoding SREBP1) promoter contains SREs, increased nSREBP1 induced a feed-forward transcription of SREBP1 (DeBose-Boyd and Ye, 2018). We found that orally gavaged LPS increased hepatic LPS, nSREBP1 abundance, and the expression of nSREBP1's target genes in *Aoah*$^{+/+}$ mice, suggesting that gut-derived LPS reaches the liver and promotes fatty acid synthesis. Thus, our data suggest that when AOAH is lacking, excessive gut-derived LPS stimulates SREBP1 activation to promote *de novo* lipogenesis in the liver, contributing to more severe MASLD.

Notably, AKT-mTOR-S6K activity increased in *Aoah*$^{-/-}$ mouse livers, which may contribute to increased SREBP1 translocation and processing (DeBose-Boyd and Ye, 2018; Jeon et al., 2023b; Owen et al., 2012). When we isolated primary mouse hepatocytes and stimulated them with LPS in vitro, we found that nSREBP1 upregulation was induced in a mTOR dependent manner, suggesting that LPS stimulates hepatocyte directly to promote mTOR activation, which induces lipid accumulation.

In addition to fatty acid biosynthesis gene expression, the expression of CD36, which is involved in free fatty acid uptake (Chen et al., 2022), also increased in the livers of young *Aoah*$^{-/-}$ mice while expression of fatty acid oxidation-related genes Acot 2 and Ppar-α decreased (Bougarne et al., 2018; Moffat et al., 2014) . In addition to taking up fatty acids, CD36 interacts with INSIG2, a negative regulator of SREBP1, promoting the translocation of SREBP1 from ER to Golgi for cleavage and activation (Zeng et al.,

2022). In keeping with our findings, Kim et al., found that LPS suppressed PPAR-α expression via ERK activation and HNF4 phosphorylation in primary mouse hepatocyte culture (Kim et al., 2024). In addition to promoting hepatic FA oxidation, PPAR-α is a transactivating factor that enhances Insig2 expression in hepatocytes, preventing SREBP activation (Lee et al., 2017). These results suggest that hepatic LPS stimulation promotes lipid accumulation via many mechanisms. In a previous study, Huang et al., found that LPS and other TLR agonists promoted fat retention in murine macrophages by increasing triacylglycerol synthesis and reducing lipolysis, yet fatty acid synthesis gene abundance did not change (Huang et al., 2014). In contrast, we found that *Aoah*$^{-/-}$ and *Aoah*$^{+/+}$ mouse livers had similar levels of Acsl1, Dgat2 and Atgl mRNAs, suggesting that in response to LPS or other PAMPs, hepatocytes and macrophages may accumulate fat via different mechanisms. Notably, we found previously that after LPS stimulation of macrophages *in vitro*, the culture medium became acidic due to aerobic glycolysis (the Warburg effect). The acidic environment contributed more to increasing fat accumulation than did LPS stimulation (Lu et al., 2014). A sensitive pH indicator is needed to find out if the blood and/or extracellular fluid in the liver become acidic due to excessive LPS stimulation and if the acidity promotes hepatic fat accumulation.

In addition to LPS, AOAH also deacylates and inactivates oxidized phospholipids and lysophospholipids (Zou et al., 2021), DAMP (Danger-Associated Molecular Pattern) molecules that are induced by inflammation and known to contribute to MASLD (Sun et al., 2020; Wang et al., 2022). By inactivating gut-derived PAMPs and DAMPs, AOAH

may decrease hepatic fat accumulation and prevent MASLD. Increasing AOAH abundance may be a useful way to prevent and/or reduce this common disease.

Data availability

All data are contained within the manuscript and the supplementary files. The RNA-seq data were deposited at PRJNA1022016.

Acknowledgments

We thank She Chen and Yanyong Xu for very helpful discussions.

References

Albillos, A., A. de Gottardi, and M. Rescigno. 2020. The gut-liver axis in liver disease: Pathophysiological basis for therapy. *Journal of hepatology* 72:558-577.

An, L., U. Wirth, D. Koch, M. Schirren, M. Drefs, D. Koliogiannis, H. Niess, J. Andrassy, M. Guba, A.V. Bazhin, J. Werner, and F. Kuhn. 2022. The Role of Gut-Derived Lipopolysaccharides and the Intestinal Barrier in Fatty Liver Diseases. *Journal of gastrointestinal surgery : official journal of the Society for Surgery of the Alimentary Tract* 26:671-683.

Anhe, F.F., N.G. Barra, J.F. Cavallari, B.D. Henriksbo, and J.D. Schertzer. 2021. Metabolic endotoxemia is dictated by the type of lipopolysaccharide. *Cell reports* 36:109691.

Aron-Wisnewsky, J., C. Vigliotti, J. Witjes, P. Le, A.G. Holleboom, J. Verheij, M. Nieuwdorp, and K. Clement. 2020a. Gut microbiota and human NAFLD: disentangling microbial signatures from metabolic disorders. *Nature reviews. Gastroenterology & hepatology* 17:279-297.

Aron-Wisnewsky, J., M.V. Warmbrunn, M. Nieuwdorp, and K. Clement. 2020b. Nonalcoholic Fatty Liver Disease: Modulating Gut Microbiota to Improve Severity? *Gastroenterology* 158:1881-1898.

Bougarne, N., B. Weyers, S.J. Desmet, J. Deckers, D.W. Ray, B. Staels, and K. De Bosscher. 2018. Molecular Actions of PPARalpha in Lipid Metabolism and Inflammation. *Endocr Rev* 39:760-802.

Carpino, G., M. Del Ben, D. Pastori, R. Carnevale, F. Baratta, D. Overi, H. Francis, V. Cardinale, P. Onori, S. Safarikia, V. Cammisotto, D. Alvaro, G. Svegliati-Baroni, F. Angelico, E. Gaudio, and F. Violi. 2020. Increased Liver Localization of Lipopolysaccharides in Human and Experimental NAFLD. *Hepatology* 72:470-485.

Charni-Natan, M., and I. Goldstein. 2020. Protocol for Primary Mouse Hepatocyte Isolation. *STAR Protoc* 1:100086.

Chen, Y., J. Zhang, W. Cui, and R.L. Silverstein. 2022. CD36, a signaling receptor and fatty acid transporter that regulates

immune cell metabolism and fate. *The Journal of experimental medicine* 219:

Cheng, X., W. Jiang, Y. Chen, B. Zou, Z. Wang, L. Gan, Z. Xiao, C. Li, C.Y. Yu, Y. Lu, Z. Han, J. Zeng, J. Gu, T. Chu, M. Fu, Y. Chu, W. Zhang, J. Tang, and M. Lu. 2023. Acyloxyacyl hydrolase promotes pulmonary defense by preventing alveolar macrophage tolerance. *PLoS pathogens* 19:e1011556.

d'Hennezel, E., S. Abubucker, L.O. Murphy, and T.W. Cullen. 2017. Total Lipopolysaccharide from the Human Gut Microbiome Silences Toll-Like Receptor Signaling. *mSystems* 2:

Daemen, S., M.M. Chan, and J.D. Schilling. 2021. Comprehensive analysis of liver macrophage composition by flow cytometry and immunofluorescence in murine NASH. *STAR Protoc* 2:100511.

DeBose-Boyd, R.A., and J. Ye. 2018. SREBPs in Lipid Metabolism, Insulin Signaling, and Beyond. *Trends Biochem Sci* 43:358-368.

Diehl, A.M., and C. Day. 2017. Cause, Pathogenesis, and Treatment of Nonalcoholic Steatohepatitis. *The New England journal of medicine* 377:2063-2072.

Fan, J.G., S.U. Kim, and V.W. Wong. 2017. New trends on obesity and NAFLD in Asia. *Journal of hepatology* 67:862-873.

Friedman, S.L., B.A. Neuschwander-Tetri, M. Rinella, and A.J. Sanyal. 2018. Mechanisms of NAFLD development and therapeutic strategies. *Nature medicine* 24:908-922.

Han, Y.H., E.J. Onufer, L.H. Huang, R.W. Sprung, W.S. Davidson, R.S. Czepielewski, M. Wohltmann, M.G. Sorci-Thomas, B.W. Warner, and G.J. Randolph. 2021. Enterically derived high-density lipoprotein restrains liver injury through the portal vein. *Science* 373:

Horton, J.D., J.L. Goldstein, and M.S. Brown. 2002. SREBPs: activators of the complete program of cholesterol and fatty acid synthesis in the liver. *The Journal of clinical investigation* 109:1125-1131.

Huang, Y.L., J. Morales-Rosado, J. Ray, T.G. Myers, T. Kho, M. Lu, and R.S. Munford. 2014. Toll-like receptor agonists promote prolonged triglyceride storage in macrophages. *The Journal of biological chemistry* 289:3001-3012.

Janelsins, B.M., M. Lu, and S.K. Datta. 2014. Altered inactivation of commensal LPS due to acyloxyacyl hydrolase deficiency in colonic dendritic cells impairs mucosal Th17 immunity. *Proceedings of the National Academy of Sciences of the United States of America* 111:373-378.

Jeon, Y.G., Y.Y. Kim, G. Lee, and J.B. Kim. 2023a. Physiological and pathological roles of lipogenesis. *Nature Metabolism* 5:735-759.

Jeon, Y.G., Y.Y. Kim, G. Lee, and J.B. Kim. 2023b. Physiological and pathological roles of lipogenesis. *Nat Metab* 5:735-759.

Ju, U.I., D.W. Jeong, J. Seo, J.B. Park, J.W. Park, K.S. Suh, J.B. Kim, and Y.S. Chun. 2020. Neddylation of sterol regulatory element-binding protein 1c is a potential therapeutic target for nonalcoholic fatty liver treatment. *Cell death & disease* 11:283.

Jump, D.B., S. Tripathy, and C.M. Depner. 2013. Fatty Acid-Regulated Transcription Factors in the Liver. *Annual Review of Nutrition, Vol 33* 33:249-269.

Kawano, Y., and D.E. Cohen. 2013. Mechanisms of hepatic triglyceride accumulation in non-alcoholic fatty liver disease. *J Gastroenterol* 48:434-441.

Kazankov, K., S.M.D. Jorgensen, K.L. Thomsen, H.J. Moller, H. Vilstrup, J. George, D. Schuppan, and H. Gronbaek. 2019. The role of macrophages in nonalcoholic fatty liver disease and nonalcoholic steatohepatitis. *Nature reviews. Gastroenterology & hepatology* 16:145-159.

Kim, G., Z. Chen, J. Li, J. Luo, F. Castro-Martinez, J. Wisniewski, K. Cui, Y. Wang, J. Sun, X. Ren, S.E. Crawford, S.P. Becerra, J. Zhu, T. Liu, S. Wang, K. Zhao, and C. Wu. 2024. Gut-liver axis calibrates intestinal stem cell fitness. *Cell*

Kisseleva, T., and D. Brenner. 2021. Molecular and cellular mechanisms of liver fibrosis and its regression. *Nature reviews.*

Gastroenterology & hepatology 18:151-166.

Kohjima, M., N. Higuchi, M. Kato, K. Kotoh, T. Yoshimoto, T. Fujino, M. Yada, R. Yada, N. Harada, M. Enjoji, R. Takayanagi, and M. Nakamuta. 2008. SREBP-1c, regulated by the insulin and AMPK signaling pathways, plays a role in nonalcoholic fatty liver disease. *International journal of molecular medicine* 21:507-511.

Lee, J.H., H.S. Kang, H.Y. Park, Y.A. Moon, Y.N. Kang, B.C. Oh, D.K. Song, J.H. Bae, and S.S. Im. 2017. PPARalpha-dependent Insig2a overexpression inhibits SREBP-1c processing during fasting. *Sci Rep* 7:9958.

Leung, C., L. Rivera, J.B. Furness, and P.W. Angus. 2016. The role of the gut microbiota in NAFLD. *Nature reviews. Gastroenterology & hepatology* 13:412-425.

Liu, X.J., N.N. Duan, C. Liu, C. Niu, X.P. Liu, and J. Wu. 2018. Characterization of a murine nonalcoholic steatohepatitis model induced by high fat high calorie diet plus fructose and glucose in drinking water. *Laboratory investigation; a journal of technical methods and pathology* 98:1184-1199.

Lu, M., T. Kho, and R.S. Munford. 2014. Prolonged triglyceride storage in macrophages: pHo trumps pO2 and TLR4. *Journal of immunology* 193:1392-1397.

Lu, M., M. Zhang, R.L. Kitchens, S. Fosmire, A. Takashima, and R.S. Munford. 2003. Stimulus-dependent deacylation of bacterial lipopolysaccharide by dendritic cells. *The Journal of experimental medicine* 197:1745-1754.

Moffat, C., L. Bhatia, T. Nguyen, P. Lynch, M. Wang, D. Wang, O.R. Ilkayeva, X. Han, M.D. Hirschey, S.M. Claypool, and E.L. Seifert. 2014. Acyl-CoA thioesterase-2 facilitates mitochondrial fatty acid oxidation in the liver. *Journal of lipid research* 55:2458-2470.

Mouries, J., P. Brescia, A. Silvestri, I. Spadoni, M. Sorribas, R. Wiest, E. Mileti, M. Galbiati, P. Invernizzi, L. Adorini, G. Penna, and M. Rescigno. 2019. Microbiota-driven gut vascular barrier disruption is a prerequisite for non-alcoholic steatohepatitis development. *Journal of hepatology* 71:1216-1228.

Munford, R.S. 1978. Endotoxin(s) and the liver. *Gastroenterology* 75:532-535.

Munford, R.S., J.P. Weiss, and M. Lu. 2020. Biochemical Transformation of Bacterial Lipopolysaccharide by acyloxyacyl hydrolase reduces host injury and promotes recovery. *The Journal of biological chemistry* 295:17842-17851.

Ojogun, N. 2008. Constitutive overexpression of Acyloxyacyl hydrolase in mus musculus. In The University of Texas Southwestern Medical Center at Dallas, Dissertation.

Ojogun, N., T.Y. Kuang, B. Shao, D.R. Greaves, R.S. Munford, and A.W. Varley. 2009. Overproduction of acyloxyacyl hydrolase by macrophages and dendritic cells prevents prolonged reactions to bacterial lipopolysaccharide in vivo. *The Journal of infectious diseases* 200:1685-1693.

Owen, J.L., Y. Zhang, S.H. Bae, M.S. Farooqi, G. Liang, R.E. Hammer, J.L. Goldstein, and M.S. Brown. 2012. Insulin stimulation of SREBP-1c processing in transgenic rat hepatocytes requires p70 S6-kinase. *Proceedings of the National Academy of Sciences of the United States of America* 109:16184-16189.

Qian, G., W. Jiang, B. Zou, J. Feng, X. Cheng, J. Gu, T. Chu, C. Niu, R. He, Y. Chu, and M. Lu. 2018. LPS inactivation by a host lipase allows lung epithelial cell sensitization for allergic asthma. *The Journal of experimental medicine* 215:2397-2412.

Ramachandran, P., R. Dobie, J.R. Wilson-Kanamori, E.F. Dora, B.E.P. Henderson, N.T. Luu, J.R. Portman, K.P. Matchett, M. Brice, J.A. Marwick, R.S. Taylor, M. Efremova, R. Vento-Tormo, N.O. Carragher, T.J. Kendall, J.A. Fallowfield, E.M. Harrison, D.J. Mole, S.J. Wigmore, P.N. Newsome, C.J. Weston, J.P. Iredale, F. Tacke, J.W. Pollard, C.P. Ponting, J.C. Marioni, S.A. Teichmann, and N.C. Henderson. 2019. Resolving the fibrotic niche of human liver cirrhosis at single-cell level. *Nature* 575:512-518.

Remmerie, A., L. Martens, T. Thone, A. Castoldi, R. Seurinck, B. Pavie, J. Roels, B. Vanneste, S. De Prijck, M. Vanhockerhout,

M. Binte Abdul Latib, L. Devisscher, A. Hoorens, J. Bonnardel, N. Vandamme, A. Kremer, P. Borghgraef, H. Van Vlierberghe, S. Lippens, E. Pearce, Y. Saeys, and C.L. Scott. 2020. Osteopontin Expression Identifies a Subset of Recruited Macrophages Distinct from Kupffer Cells in the Fatty Liver. *Immunity* 53:641-657 e614.

Rodrigues, S.G., S. van der Merwe, A. Krag, and R. Wiest. 2024. Gut-liver axis: Pathophysiological concepts and medical perspective in chronic liver diseases. *Seminars in Immunology* 71:

Shao, B., R.L. Kitchens, R.S. Munford, T.E. Rogers, D.C. Rockey, and A.W. Varley. 2011. Prolonged hepatomegaly in mice that cannot inactivate bacterial endotoxin. *Hepatology* 54:1051-1062.

Shao, B., M. Lu, S.C. Katz, A.W. Varley, J. Hardwick, T.E. Rogers, N. Ojogun, D.C. Rockey, R.P. Dematteo, and R.S. Munford. 2007. A host lipase detoxifies bacterial lipopolysaccharides in the liver and spleen. *The Journal of biological chemistry* 282:13726-13735.

Sheka, A.C., O. Adeyi, J. Thompson, B. Hameed, P.A. Crawford, and S. Ikramuddin. 2020. Nonalcoholic Steatohepatitis: A Review. *Jama* 323:1175-1183.

Shimano, H., and R. Sato. 2017. SREBP-regulated lipid metabolism: convergent physiology - divergent pathophysiology. *Nature reviews. Endocrinology* 13:710-730.

Su, G.L. 2002. Lipopolysaccharides in liver injury: molecular mechanisms of Kupffer cell activation. *Am J Physiol Gastrointest Liver Physiol* 283:G256-265.

Sun, X., J.S. Seidman, P. Zhao, T.D. Troutman, N.J. Spann, X. Que, F. Zhou, Z. Liao, M. Pasillas, X. Yang, J.A. Magida, T. Kisseleva, D.A. Brenner, M. Downes, R.M. Evans, A.R. Saltiel, S. Tsimikas, C.K. Glass, and J.L. Witztum. 2020. Neutralization of Oxidized Phospholipids Ameliorates Non-alcoholic Steatohepatitis. *Cell metabolism* 31:189-206 e188.

Wang, H., S.T. Reddy, and A.M. Fogelman. 2022. The role of gut-derived oxidized lipids and bacterial lipopolysaccharide in systemic inflammation and atherosclerosis. *Current opinion in lipidology*

Ye, D., F.Y. Li, K.S. Lam, H. Li, W. Jia, Y. Wang, K. Man, C.M. Lo, X. Li, and A. Xu. 2012. Toll-like receptor-4 mediates obesity-induced non-alcoholic steatohepatitis through activation of X-box binding protein-1 in mice. *Gut* 61:1058-1067.

Yecies, J.L., H.H. Zhang, S. Menon, S. Liu, D. Yecies, A.I. Lipovsky, C. Gorgun, D.J. Kwiatkowski, G.S. Hotamisligil, C.H. Lee, and B.D. Manning. 2011. Akt stimulates hepatic SREBP1c and lipogenesis through parallel mTORC1-dependent and independent pathways. *Cell metabolism* 14:21-32.

Yokoyama, C., X. Wang, M.R. Briggs, A. Admon, J. Wu, X. Hua, J.L. Goldstein, and M.S. Brown. 1993. SREBP-1, a basic-helix-loop-helix-leucine zipper protein that controls transcription of the low density lipoprotein receptor gene. *Cell* 75:187-197.

Younossi, Z., Q.M. Anstee, M. Marietti, T. Hardy, L. Henry, M. Eslam, J. George, and E. Bugianesi. 2018. Global burden of NAFLD and NASH: trends, predictions, risk factors and prevention. *Nature reviews. Gastroenterology & hepatology* 15:11-20.

Yu, J., C. Zhu, X. Wang, K. Kim, A. Bartolome, P. Dongiovanni, K.P. Yates, L. Valenti, M. Carrer, T. Sadowski, L. Qiang, I. Tabas, J.E. Lavine, and U.B. Pajvani. 2021. Hepatocyte TLR4 triggers inter-hepatocyte Jagged1/Notch signaling to determine NASH-induced fibrosis. *Science translational medicine* 13:

Zeng, H., H. Qin, M. Liao, E. Zheng, X. Luo, A. Xiao, Y. Li, L. Chen, L. Wei, L. Zhao, X.Z. Ruan, P. Yang, and Y. Chen. 2022. CD36 promotes de novo lipogenesis in hepatocytes through INSIG2-dependent SREBP1 processing. *Molecular metabolism* 57:101428.

Zou, B., M. Goodwin, D. Saleem, W. Jiang, J. Tang, Y. Chu, R.S. Munford, and M. Lu. 2021. A highly conserved host lipase deacylates oxidized phospholipids and ameliorates acute lung injury in mice. *Elife* 10:

Figure 1. AOAH reduces hepatic lipid accumulation.

(A) AOAH cleaves the two piggyback fatty acyl chains from the lipid A moiety, inactivating LPS. The arrows indicate the cleavage sites.

(B) Co-housed *Aoah*$^{+/+}$ and *Aoah*$^{-/-}$ mice were fed either a normal diet (NC) or a high fat diet plus high fructose (23.1 g/L) and glucose (18.9 g/L) in their drinking water (HFD) for 28 weeks.

(C) Body weight was measured weekly for 28 weeks. Data were combined from 4 experiments. n = 12 – 17.

(D) Representative images of livers at 28 weeks are shown and the liver weight was measured. n = 7 – 9.

(E) Mouse livers were fixed, sectioned and stained with Oil Red O or Hematoxylin-eosin (H & E). In Oil Red O-stained sections, the percentage of area occupied by the lipid droplets was quantified using Image J. H & E staining results were semi-quantitatively scored for disease severity. Data were combined from 3 experiments, n = 6. Scare bars = 100 μm.

(F) Triacylglycerol (TAG) and total cholesterol (TCHO) were measured in liver homogenates. Data were combined from at 3 experiments, n = 9 – 11.

(G) The serum concentrations of triglyceride, total cholesterol, HDL, LDL and free fatty acids were measured. Data were combined from 3 experiments. n = 4 – 10.

(C - G) Mann-Whitney test and Two-way ANOVA test were used. *, $P < 0.05$; **, $P < 0.01$; ***, $P < 0.001$.

Figure 2. AOAH prevents hepatic inflammation and tissue injury when mice are fed HFD.

(A) Serum ALT and AST were measured at 28 weeks. Data were combined from 3 experiments, n = 7 – 12.

(B-C) Inflammation-related *Tnf-α, Il-6, Ifn-γ, Il-10* mRNA and fibrosis-related *Timp1, Mmp2, α-SMA, Collagen 4α1* mRNA were measured in livers at 28 weeks. Data were combined from 3 experiments, n = 6 – 10.

(D) Gating strategy to identify hepatic neutrophils, monocytes, Kupffer cells, lipid-associated macrophages (LAM) and monocyte-derived Kupffer cells (Mo-KC) subsets.

(E) The myeloid cell numbers in *Aoah*$^{+/+}$ and *Aoah*$^{-/-}$ livers were calculated using FACS analysis. Data were combined from 3 experiments, n = 6 – 8. Mann-Whitney test was used. *, $P < 0.05$; **, $P < 0.01$.

Figure 3. AOAH reduces hepatic LPS levels and the expression of fatty acid uptake and synthesis genes.

(A) AOAH expression in mouse hepatic cells based on single cell analysis by Remmerie et al. (Remmerie et al., 2020) is shown, n = 4.

(B) Kupffer cells, monocytes and NK cells were sorted using flow cytometry and hepatocytes were purified from 6 - 8 weeks old mice. AOAH mRNA was measured. Data were combined from 3 experiments, n = 7 – 8.

(C) Using Western blot analysis, we confirmed that AOAH protein was present in 6 –8-week-old *Aoah*$^{+/+}$ mouse livers but not in *Aoah*$^{-/-}$ mouse liver homogenates. Similar results were obtained in two other experiments.

(D) AOAH mRNA levels in the livers of *Aoah*$^{+/+}$ mice fed with a normal chow for 8 and 28 weeks, and a high-fat diet for 28 weeks were measured. Data were combined from 3 experiments, n = 8 – 9.

(E) Single-cell RNA sequencing data from livers of MASLD patients and healthy controls by Ramachandran et al. are shown (Ramachandran et al., 2019). n = 5/group.

(F) Heat-inactivated feces suspension, liver homogenates and plasma from *Aoah*$^{+/+}$ and *Aoah*$^{-/-}$ mice were tested for TLR4-stimulating activity. Data were combined from at least 3 experiments, n = 6 – 10.

(G) Gut permeability was measured. Mice were fasted for 18 h. Mice were orally gavaged with fluorescein isothiocyanate (FITC)-conjugated dextran and 4 h later, FITC fluorescence was measured in plasma. Data were combined from 3 experiments, n = 5 – 7.

(H) At 28 weeks of NC or HFD feeding, liver *Fabp3* and *Fasn* mRNAs were measured. Data were combined from 3 experiments, n = 8 – 11.

Mann-Whitney test was used. *, $P < 0.05$; **, $P < 0.01$.

Figure 4. AOAH regulates the expression of hepatic fatty acid metabolism genes.

(A-B) Co-housed 6 – 8 weeks old (i.e. young) *Aoah*$^{+/+}$ and *Aoah*$^{-/-}$ mouse livers were subjected to RNAseq analysis. The differentially expressed genes are shown in the volcano plot (A). The fatty acid biosynthesis pathway was found enriched using GSEA (Gene set enrichment analysis) (B, left panel). The fatty acid biosynthesis-associated gene expression levels of co-housed *Aoah*$^{+/+}$ and *Aoah*$^{-/-}$ mouse livers are shown as a heatmap, n = 4 (B, middle panel). The fatty acid biosynthesis pathway is shown. The enzymes marked red had increased expression in young *Aoah*$^{-/-}$ mouse livers (B, right panel).

(C-E) The hepatic expression of fatty acid synthesis (C), oxidation (D) and uptake (E) genes was measured in co-housed 6 – 8 week-old *Aoah*$^{+/+}$ and *Aoah*$^{-/-}$ mice. Data were combined from 3 experiments, n = 5 – 8.

(F) Liver homogenates from co-housed 6 – 8 weeks old *Aoah*$^{+/+}$ and *Aoah*$^{-/-}$ mice were subjected to Western blot analysis. FASN, SCD1 and α-Tubulin protein levels were quantitated using Image J. Data were combined from 2 experiments, n = 6.

Mann-Whitney test was used. *, $P < 0.05$; **, $P < 0.01$.

Figure 5. AOAH reduces hepatic SREBP1.

(A) *SREBP-1a* and *SREBP-1c* gene mRNA was measured in livers from *Aoah*$^{+/+}$ and *Aoah*$^{-/-}$ mice. n = 8.

(B) Liver homogenates from *Aoah*$^{+/+}$ and *Aoah*$^{-/-}$ mice were subjected to Western blot analysis. SREBP1 protein levels were quantitated using Image J. flSREBP1 is full

length SREBP1, which is a precursor; nSREBP1is nuclear SREBP1, which is an active form. n = 4 – 6.

(C) Liver cytosol and nuclei were separated from *Aoah*$^{+/+}$ and *Aoah*$^{-/-}$ mice and then subjected to Western blot analysis. SREBP1 protein levels were quantitated using Image J. n = 6.

(D) *Aoah*$^{+/+}$ mice were injected i.v. with 200 μl clodronate-liposomes or PBS-liposomes. After 2 days, livers were dissected, sectioned and stained with anti-F4/80 antibody (white) and DAPI (blue). AOAH mRNA was measured in livers. SREBP1, pAKT, AKT, pmTOR and mTOR were measured using Western blotting. n = 6.

Mann-Whitney test was used. *, $P < 0.05$; **, $P < 0.01$.

Figure 6. Excessive gut-derived LPS increases hepatic nSREBP1 and mTOR activation.

Livers from *Aoah*$^{+/+}$mice, *Aoah*$^{-/-}$ mice and *Aoah*$^{+/+}$ mice that were orally gavaged (i.g.) with 200 μg LPS 24 h earlier were obtained.

(A) Hepatic LPS levels were measured.

(B) *SREBP-1a* and *SREBP-1c* mRNA was measured in livers.

(C) The mRNA levels of fatty acid biosynthesis-related genes and CD36 were measured using qPCR. (A-C) Data were combined from 2 experiments, n = 5 – 7.

(D) SREBP1 protein levels and AKT-mTOR activities were measured using Western blot and Image J. Livers from *Aoah*$^{-/-}$ mice and *Aoah*$^{+/+}$ mice that were orally gavaged

(i.g.) with 200 μg LPS 24 h earlier had increased nSREBP1 and mTOR activities than did those from control *Aoah*$^{+/+}$ mice. Data were combined from 2 experiments, n = 6.

(E) Primary hepatocytes were isolated from co-housed 6 – 8 weeks old *Aoah*$^{+/+}$ mice and treated with 10 ng/ml LPS with or without 100 nM Torin1 for 6 h. Cells were lysed for Western blot analysis. n = 3. The same experiment was repeated twice with similar results.

Mann-Whitney test was used. *, $P < 0.05$; **, $P < 0.01$; ***, $P < 0.001$.

Figure 7. AOAH prevents MASLD by inactivating gut-derived LPS.

Gut-derived LPS may translocate via the portal vein to the liver. In *Aoah*$^{+/+}$ mice, LPS can be deacylated by AOAH in the intestine and portal venous blood; when intact LPS reaches the liver it can be inactivated by hepatic AOAH. In *Aoah*$^{-/-}$ mice, gut-derived LPS remains able to stimulate fat accumulation (steatosis) in the liver. LPS stimulates hepatocytes to generate nuclear SREBP1, which promotes fatty acid biosynthesis gene expression. LPS also increases the expression of fatty acid uptake genes CD36 and Fabp3 while reducing that of fatty acid oxidation related genes, Acot2 and Ppar-α. Persistent LPS stimulation renders *Aoah*$^{-/-}$ mice more likely to develop MASLD than are *Aoah*$^{+/+}$ mice. dLPS = deacylated LPS.

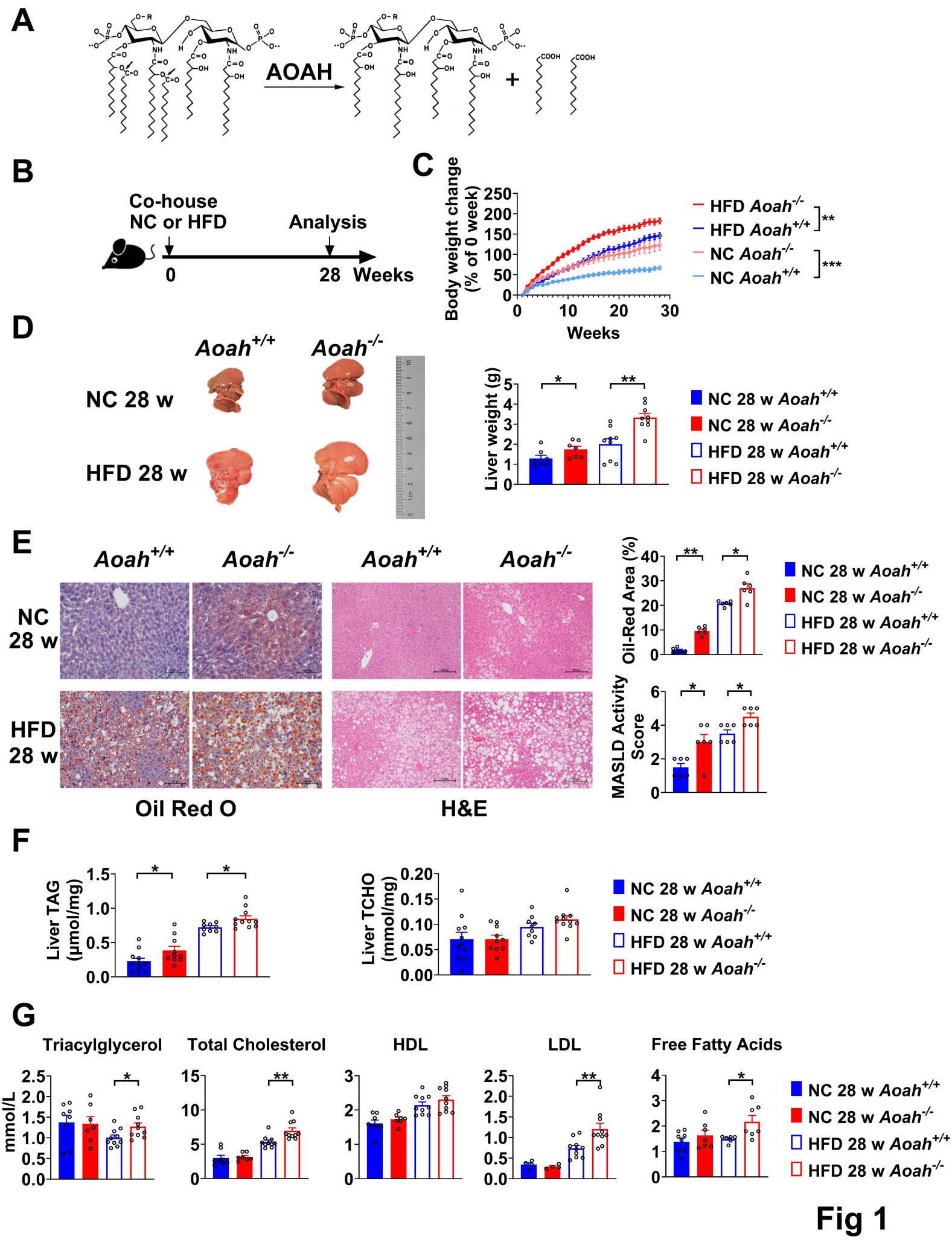
A
AOAH
B
Co-house
NC or HFD
Analysis
0
28 Weeks
C
Body weight change (% of 0 week)
Weeks
HFD Aoah-/-
HFD Aoah+/+
NC Aoah-/-
NC Aoah+/+
**
***
D
Aoah+/+
Aoah-/-
NC 28 w
HFD 28 w
Liver weight (g)
NC 28 w Aoah+/+
NC 28 w Aoah-/-
HFD 28 w Aoah+/+
HFD 28 w Aoah-/-
E
Oil Red O
H&E
Oil-Red Area (%)
MASLD Activity Score
F
Liver TAG (μmol/mg)
Liver TCHO (mmol/mg)
G
Triacylglycerol
Total Cholesterol
HDL
LDL
Free Fatty Acids
mmol/L

Fig 1

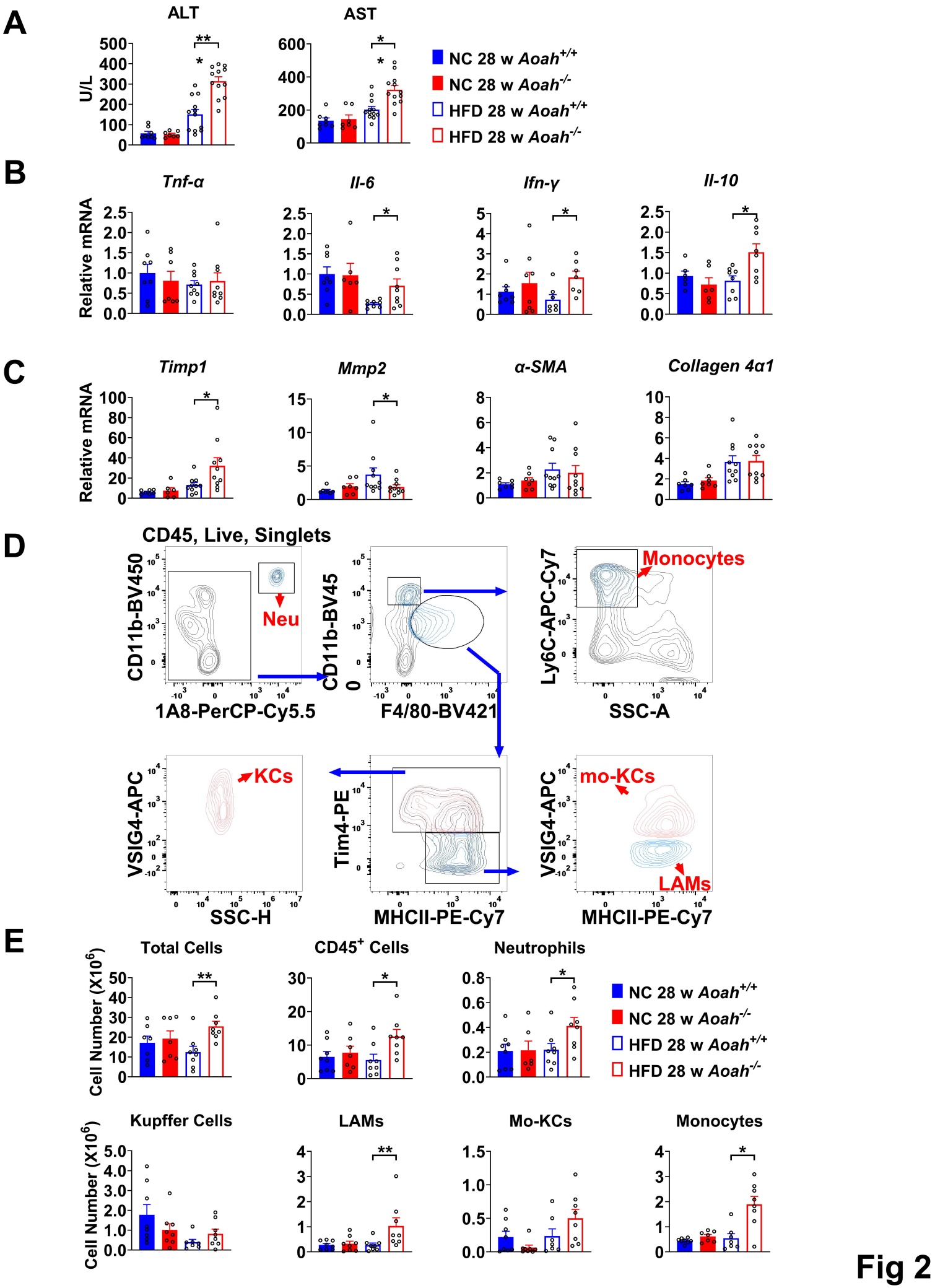
A
ALT
AST
U/L
NC 28 w Aoah+/+
NC 28 w Aoah-/-
HFD 28 w Aoah+/+
HFD 28 w Aoah-/-
B
Tnf-α
Il-6
Ifn-γ
Il-10
Relative mRNA
C
Timp1
Mmp2
α-SMA
Collagen 4α1
Relative mRNA
D
CD45, Live, Singlets
CD11b-BV450
1A8-PerCP-Cy5.5
Neu
CD11b-BV45
F4/80-BV421
Ly6C-APC-Cy7
SSC-A
Monocytes
VSIG4-APC
SSC-H
KCs
Tim4-PE
MHCII-PE-Cy7
mo-KCs
LAMs
E
Total Cells
CD45+ Cells
Neutrophils
Cell Number (X10^6)
Kupffer Cells
LAMs
Mo-KCs
Monocytes

Fig 2

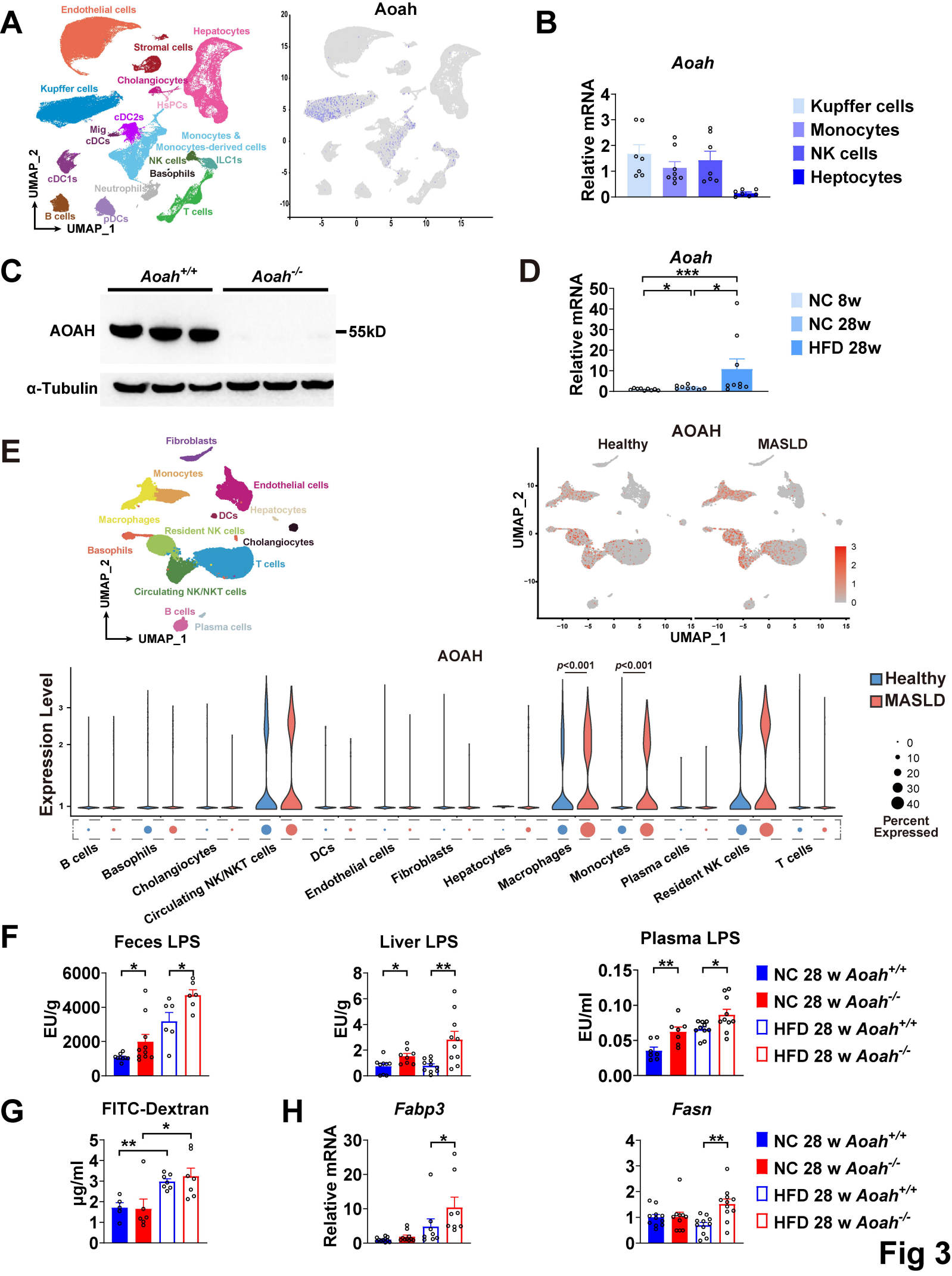
A
Endothelial cells
Hepatocytes
Stromal cells
Cholangiocytes
Kupffer cells
HSPCs
cDC2s
Mig cDCs
Monocytes & Monocytes-derived cells
NK cells
ILC1s
Basophils
cDC1s
Neutrophils
B cells
pDCs
T cells
UMAP_2
UMAP_1
Aoah
B
Aoah
Relative mRNA
Kupffer cells
Monocytes
NK cells
Heptocytes
C
Aoah+/+
Aoah-/-
AOAH
55kD
α-Tubulin
D
Aoah
Relative mRNA
NC 8w
NC 28w
HFD 28w
E
Fibroblasts
Monocytes
Endothelial cells
Hepatocytes
DCs
Macrophages
Resident NK cells
Cholangiocytes
Basophils
T cells
Circulating NK/NKT cells
B cells
Plasma cells
UMAP_2
UMAP_1
AOAH
Healthy
MASLD
AOAH
Expression Level
p<0.001
p<0.001
Healthy
MASLD
Percent Expressed
B cells
Basophils
Cholangiocytes
Circulating NK/NKT cells
DCs
Endothelial cells
Fibroblasts
Hepatocytes
Macrophages
Monocytes
Plasma cells
Resident NK cells
T cells
F
Feces LPS
EU/g
Liver LPS
EU/g
Plasma LPS
EU/ml
NC 28 w Aoah+/+
NC 28 w Aoah-/-
HFD 28 w Aoah+/+
HFD 28 w Aoah-/-
G
FITC-Dextran
μg/ml
H
Fabp3
Relative mRNA
Fasn
NC 28 w Aoah+/+
NC 28 w Aoah-/-
HFD 28 w Aoah+/+
HFD 28 w Aoah-/-
Fig 3

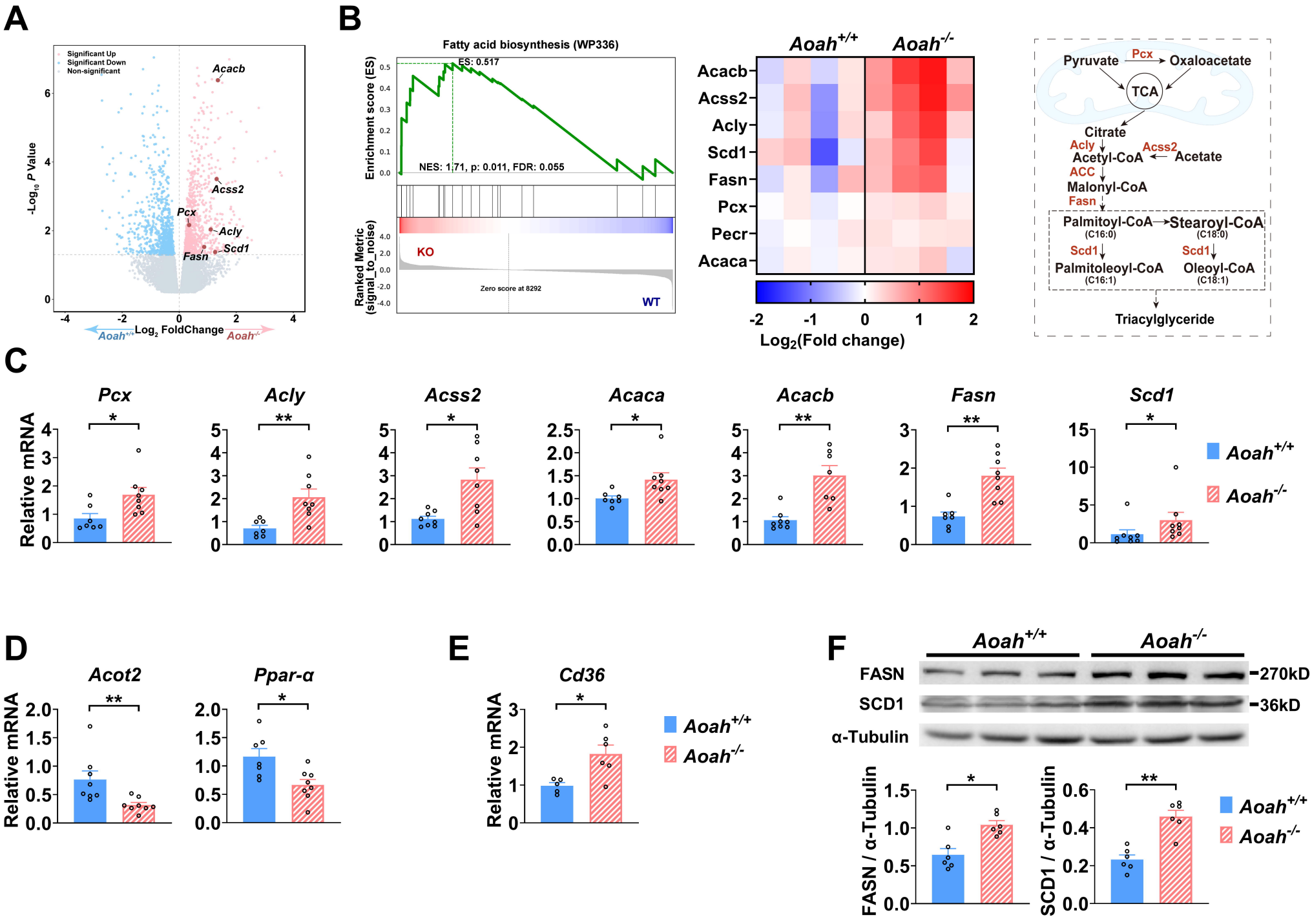
A
Significant Up
Significant Down
Non-significant
Acacb
Acss2
Pcx
Acly
Scd1
Fasn
-Log10 P Value
Log2 FoldChange
Aoah+/+
Aoah-/-
B
Fatty acid biosynthesis (WP336)
ES: 0.517
NES: 1.71, p: 0.011, FDR: 0.055
Enrichment score (ES)
Ranked Metric (signal_to_noise)
KO
WT
Zero score at 8292
Aoah+/+
Aoah-/-
Acacb
Acss2
Acly
Scd1
Fasn
Pcx
Pecr
Acaca
Log2(Fold change)
Pyruvate
Pcx
Oxaloacetate
TCA
Citrate
Acly
Acetyl-CoA
Acss2
Acetate
ACC
Malonyl-CoA
Fasn
Palmitoyl-CoA (C16:0)
Stearoyl-CoA (C18:0)
Scd1
Palmitoleoyl-CoA (C16:1)
Oleoyl-CoA (C18:1)
Triacylglyceride
C
Pcx
Acly
Acss2
Acaca
Acacb
Fasn
Scd1
Relative mRNA
Aoah+/+
Aoah-/-
D
Acot2
Ppar-α
Relative mRNA
E
Cd36
Relative mRNA
Aoah+/+
Aoah-/-
F
Aoah+/+
Aoah-/-
FASN
SCD1
α-Tubulin
270kD
36kD
FASN / α-Tubulin
SCD1 / α-Tubulin
Aoah+/+
Aoah-/-

Fig 4

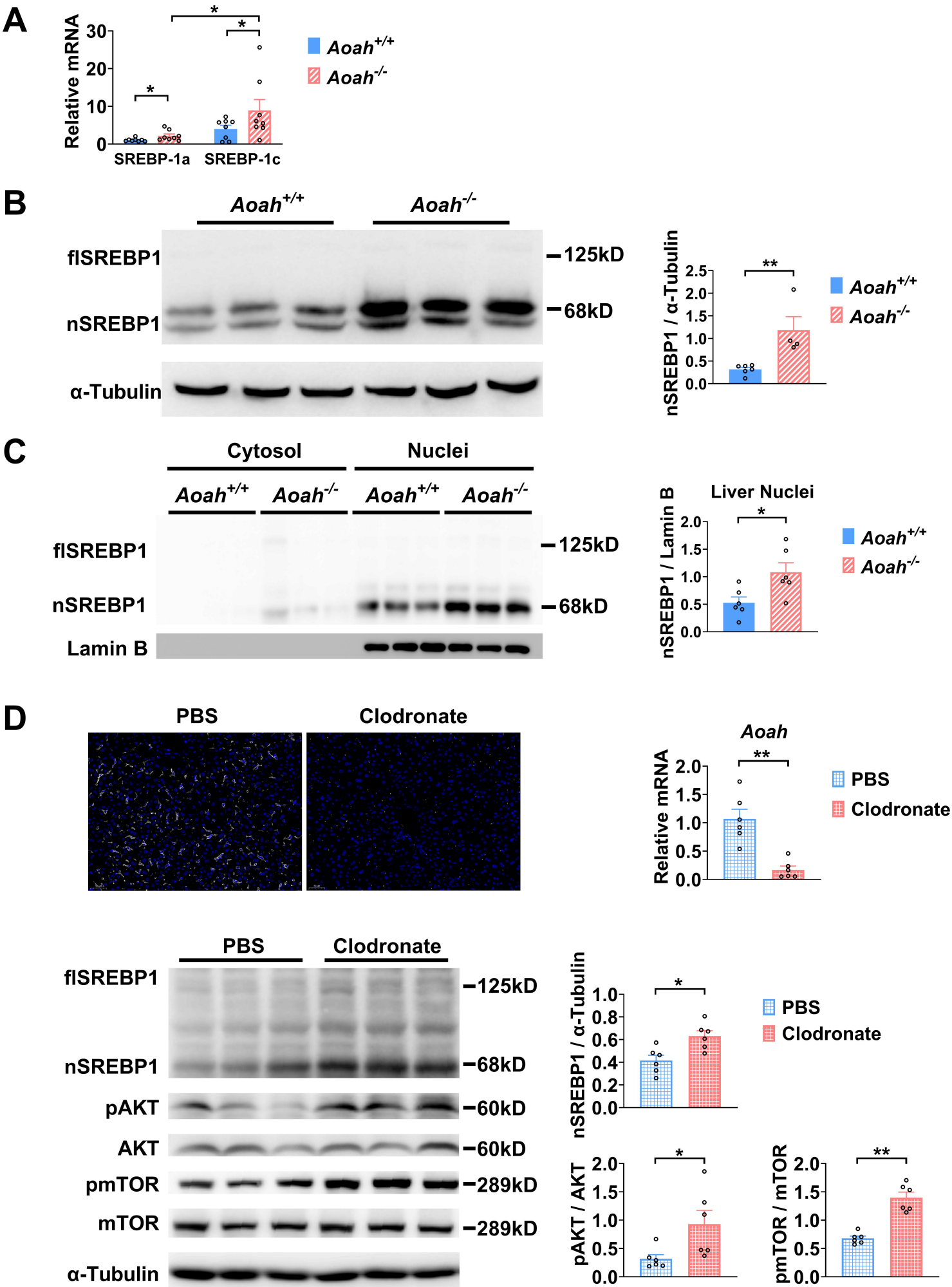
A
Relative mRNA
30
20
10
0
*
*
*
SREBP-1a
SREBP-1c
Aoah+/+
Aoah-/-
B
Aoah+/+
Aoah-/-
flSREBP1
nSREBP1
α-Tubulin
125kD
68kD
nSREBP1 / α-Tubulin
2.5
2.0
1.5
1.0
0.5
0.0
**
Aoah+/+
Aoah-/-
C
Cytosol
Nuclei
Aoah+/+
Aoah-/-
Aoah+/+
Aoah-/-
flSREBP1
nSREBP1
Lamin B
125kD
68kD
Liver Nuclei
nSREBP1 / Lamin B
2.0
1.5
1.0
0.5
0.0
*
Aoah+/+
Aoah-/-
D
PBS
Clodronate
Aoah
Relative mRNA
2.0
1.5
1.0
0.5
0.0
**
PBS
Clodronate
PBS
Clodronate
flSREBP1
nSREBP1
pAKT
AKT
pmTOR
mTOR
α-Tubulin
125kD
68kD
60kD
60kD
289kD
289kD
nSREBP1 / α-Tubulin
1.0
0.8
0.6
0.4
0.2
0.0
*
PBS
Clodronate
pAKT / AKT
2.0
1.5
1.0
0.5
0.0
*
pmTOR / mTOR
2.0
1.5
1.0
0.5
0.0
**

Fig 5

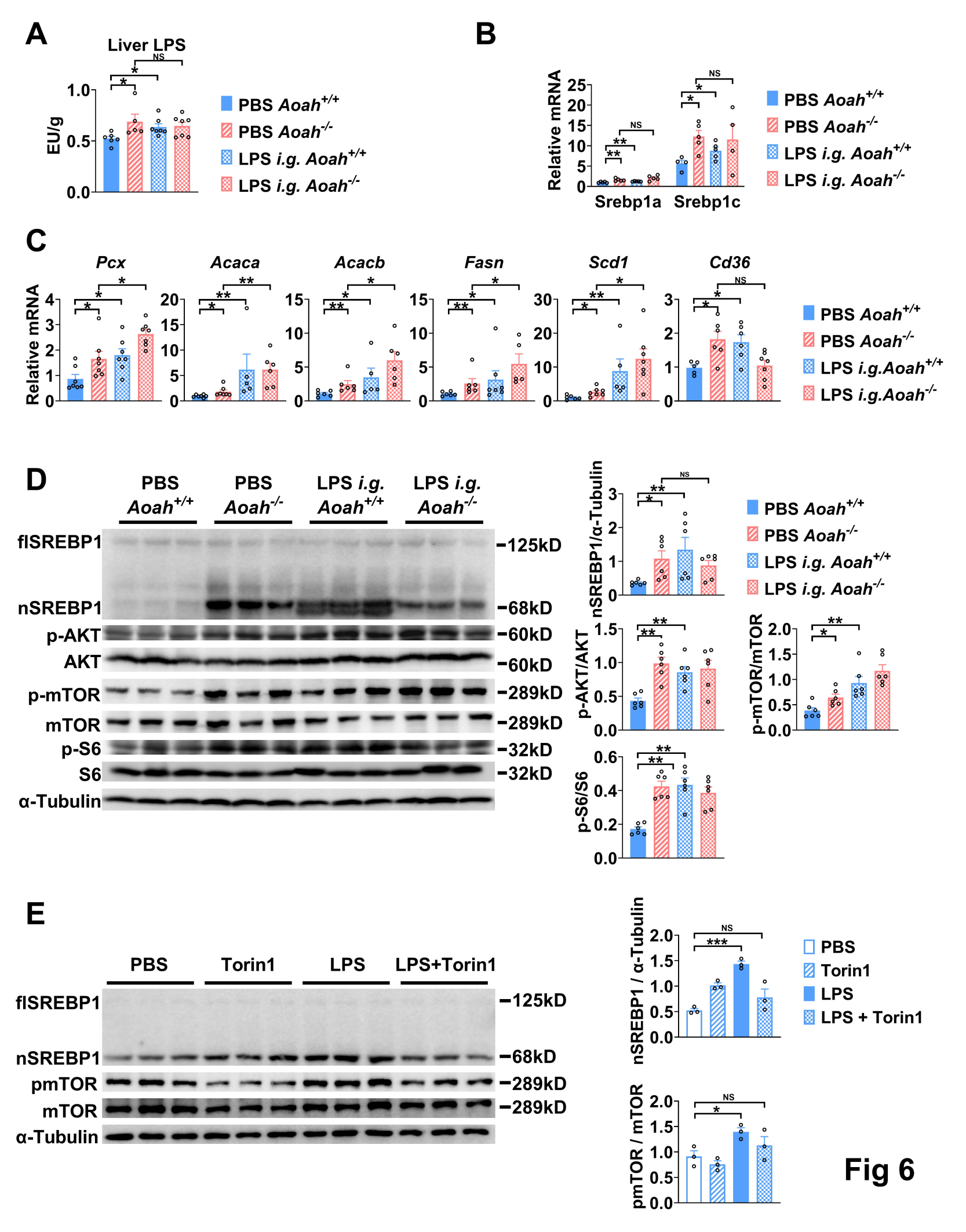
A
Liver LPS
EU/g
PBS Aoah+/+
PBS Aoah-/-
LPS i.g. Aoah+/+
LPS i.g. Aoah-/-
B
Relative mRNA
Srebp1a
Srebp1c
C
Pcx
Acaca
Acacb
Fasn
Scd1
Cd36
Relative mRNA
D
PBS Aoah+/+
PBS Aoah-/-
LPS i.g. Aoah+/+
LPS i.g. Aoah-/-
flSREBP1
nSREBP1
p-AKT
AKT
p-mTOR
mTOR
p-S6
S6
α-Tubulin
125kD
68kD
60kD
60kD
289kD
289kD
32kD
32kD
nSREBP1/α-Tubulin
p-AKT/AKT
p-mTOR/mTOR
p-S6/S6
E
PBS
Torin1
LPS
LPS+Torin1
flSREBP1
nSREBP1
pmTOR
mTOR
α-Tubulin
125kD
68kD
289kD
289kD
nSREBP1 / α-Tubulin
pmTOR / mTOR
Fig 6

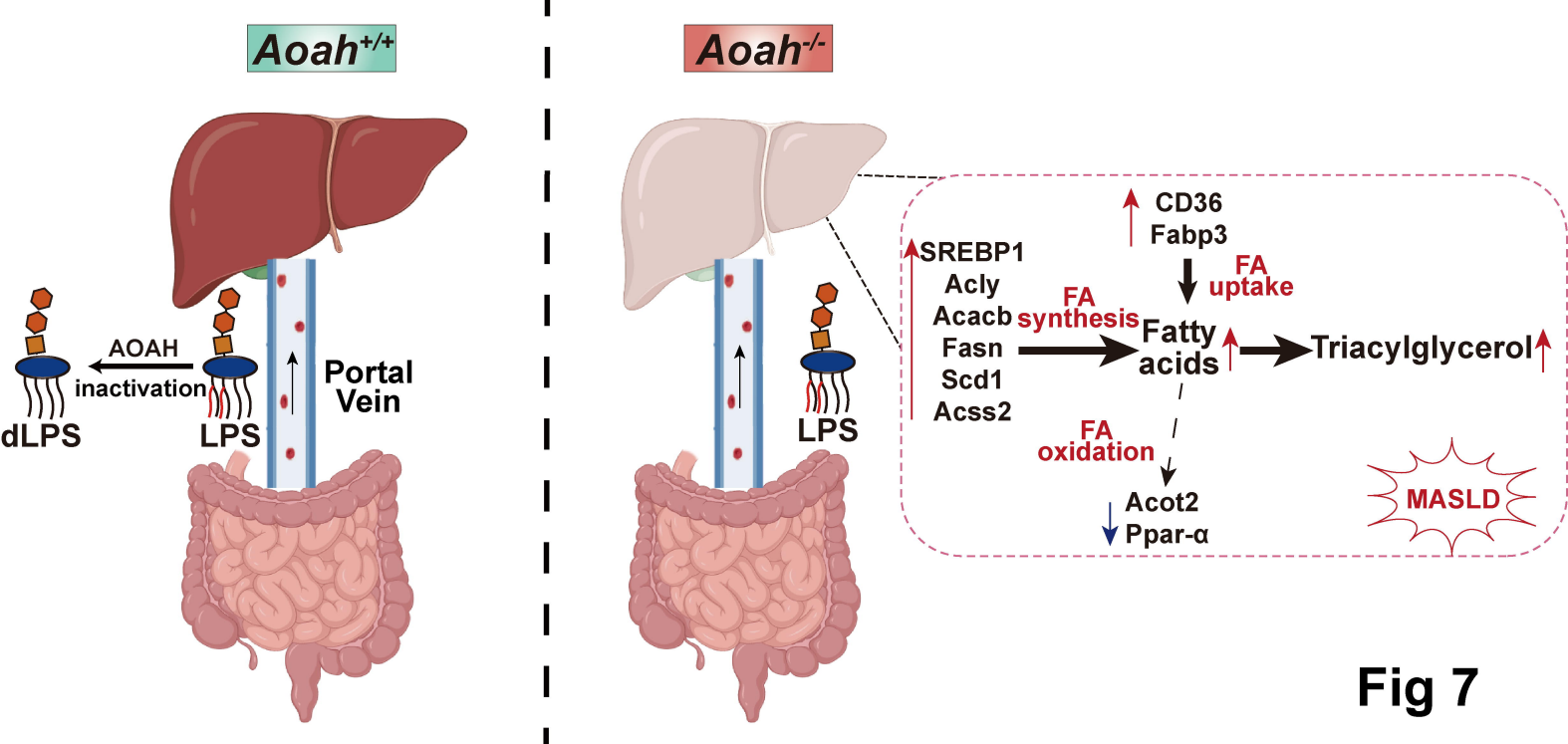
Aoah+/+
Aoah-/-
AOAH
inactivation
dLPS
LPS
Portal
Vein
LPS
CD36
Fabp3
FA
uptake
SREBP1
Acly
Acacb
Fasn
Scd1
Acss2
FA
synthesis
Fatty
acids
Triacylglycerol
FA
oxidation
Acot2
Ppar-α
MASLD

Fig 7